ACS APPLIED MATERIALS & INTERFACES

Research Article

www.acsami.org

Analysis of Nanoporosity in Moisture Permeation Barrier Layers by Electrochemical Impedance Spectroscopy

Alberto Perrotta,*[,†,‡] Santiago J. García,[§] Jasper J. Michels,[∥] Anne-Marije Andringa,[†] and Mariadriana Creatore[†,⊥]

[†]Department of Applied Physics, Eindhoven University of Technology, P.O. Box 513, 5600 MB Eindhoven, The Netherlands

[‡]Dutch Polymer Institute (DPI), P.O. Box 902, 5600 AX Eindhoven, The Netherlands

[§]Delft University of Technology, Novel Aerospace Materials, Kluyverweg 1, 2629 HS Delft, The Netherlands

[∥]Max Planck Institute for Polymer Research (MPIP), Ackermannweg 10, D-55128 Mainz, Germany

[⊥]Solar Research SOLLIANCE, High Tech Campus 21, 5656 AE Eindhoven, The Netherlands

ABSTRACT: Water permeation in inorganic moisture permeation barriers occurs through macroscale defects/pinholes and nanopores, the latter with size approaching the water kinetic diameter (0.27 nm). Both permeation paths can be identified by the calcium test, i.e., a time-consuming and expensive optical method for determining the water vapor transmission rate (WVTR) through barrier layers. Recently, we have shown that ellipsometric porosimetry (i.e., a combination of spectroscopic ellipsometry and isothermal adsorption studies) is a valid method to classify and quantify the nanoporosity and correlate it with the WVTR values. Nevertheless, no information is obtained about the macroscale defects or the kinetics of water permeation through the barrier, both essential in assessing the quality of the barrier layer. In this study, electrochemical impedance spectroscopy (EIS) is shown as a sensitive and versatile method to obtain information on nanoporosity and macroscale defects, water permeation, and diffusivity of moisture barrier layers, complementing the barrier property characterization obtained by means of EP and calcium test. EIS is performed on thin SiO_2 barrier layers deposited by plasma enhanced-CVD. It allows the determination of the relative water uptake in the SiO_2 layers, found to be in agreement with the nanoporosity content inferred by EP. Furthermore, the kinetics of water permeation is followed by EIS, and the diffusivity (D) is determined and found to be in accordance with literature values. Moreover, differently from EP, EIS data are shown to be sensitive to the presence of local macrodefects, correlated with the barrier failure during the calcium test.

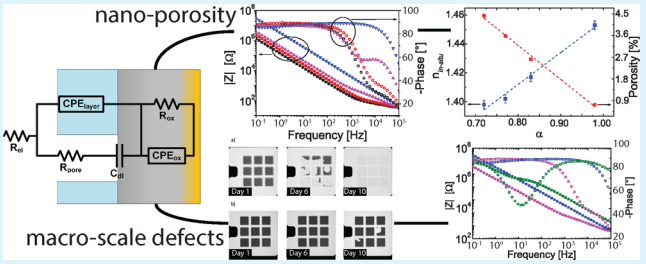

KEYWORDS: *EIS, PE-CVD, moisture permeation barrier, nanoporosity, macrodefects*

1. INTRODUCTION

Organic semiconductors represent an attractive class of active elements for several electronic and optoelectronic devices, ranging from solar cells to organic-LEDs. However, the high sensitivity of such devices to moisture and oxygen makes the application of moisture barrier layers mandatory.[1,2] Inorganic layers, such as SiO_2, Si_3N_4, Al_2O_3, and TiO_2, are good candidates because of their proven excellent barrier properties.[3−6]

The quality of the moisture barrier layer is generally classified in terms of water vapor transmission rate (WVTR), reported as the extent of water vapor permeating through the barrier per unit area in time (gm^{-2} day^{-1}). The most demanding requirement in terms of WVTR is represented by organic LED (OLED), where WVTR values on the order of 10^{-6} gm^{-2} day^{-1} should be obtained in order to guarantee a long-term device shelf life.[7,8] Water vapor transmission rate can be measured by several (commercially available) analytical tools, i.e., permeameters and optical or electrical calcium (Ca) tests.[9,10] In the optical Ca test, the oxidation of a calcium layer in contact with the barrier is used to follow the water permeation in time.

It is demonstrated that the failure of barrier layers relates with the presence of permeation pathways for water in the inorganic barrier. Moisture permeation is shown to occur through (i) macroscale (often process-induced) local pathways (with dimensions between a few nanometers up to several hundreds of micrometers in the case of pinholes/defects) and through (ii) nanopores (or free volume, with dimensions between the H_2O kinetic diameter (0.27 nm) and roughly 2 nm), characteristic of the matrix of the inorganic layer.[11−15] The barrier properties related to the permeation through the nanopores are generally addressed as *intrinsic*, while the overall permeation through both macrodefects and nanopores is addressed as the *effective* barrier property. Typically, the Ca test can be used to distinguish the two permeation pathways.

Received: May 11, 2015
Accepted: July 6, 2015
Published: July 6, 2015

DOI: 10.1021/acsami.5b04060
ACS Appl. Mater. Interfaces 2015, 7, 15968−15977

While the *effective* WVTR is given by the overall permeation, the *intrinsic* (*i*-) WVTR values are obtained by excluding the contribution of the local white spots, which develop from the permeation of water vapor through the macroscale defects.[16] Despite the fact that this test is widely accepted, it is rather time-consuming and its reproducibility is affected by the quality of the Ca plates. Moreover, the kinetics of calcium oxidation is highly dependent on the test setup, and recently its accuracy has been strongly criticized.[10] The development of techniques capable of assessing the quality of the barriers and giving information about the permeation pathways is thus of high relevance.

Recently, we have shown that the nanoporosity relative content in oxide layers measured by means of ellipsometric porosimetry (EP) correlates with the *i*-WVTR values. [The porosity is categorized according to the IUPAC classification. Mesoporous layers show pore sizes in the 2−50 nm range. Nanoporous (elsewhere also called microporous) layers show pore sizes below 2 nm. Pores with diameter larger than 50 nm characterize macroporous layers.[53]] Hence, the nanoporosity can be used to rank the *intrinsic* barrier quality and predict (*intrinsic*) barrier performances.[15] EP is based on the adsorption/desorption of a probe molecule within the matrix of a layer, followed by spectroscopic ellipsometry as changes in the layer optical properties.[15,17−21] However, no information can be obtained about macroscale defects due to their dimensions. The probe molecule uptake in a macroscale defect is measured as a multilayer development, due to the large distances of the defect walls which limits the microstructure characterization and, hence, the barrier quality classification, to the *intrinsic* properties. Furthermore, with this technique the probe molecule uptake is measured under equilibrium conditions, and, therefore, information on the kinetics of diffusion (diffusivity and permeability) of the adsorptive into thin films cannot be inferred.

In the engineering of barrier layers, the diffusion coefficient of water represents a crucial characteristic of the barrier, since the permeability (P) of a gas/vapor through a layer is given by the product of its diffusivity (D) and solubility (S). In the literature, Graff et al.[4] presented time-dependent permeation data to calculate the effective diffusivity and solubility for water vapor through a sputtered aluminum oxide barrier layer, reporting D values of 1.4×10^{-13} cm^2 s^{-1} by means of a commercially available permeameter. In another contribution, Carcia et al.[22] calculated the water diffusivity through an alumina layer deposited by atomic layer deposition (ALD) from its permeability measurement and reported a D value of 2.5×10^{-17} cm^2 s^{-1}. The determination of D gives information on the barrier performance of the layer, hence contributing to the classification of the barrier quality.

Electrochemical impedance spectroscopy (EIS) has been extensively applied for the determination of the diffusion coefficients of both thick and thin organic layers, mainly with application as anticorrosion coatings on metallic substrates.[23,24] The water permeation through a layer is followed by the changes of the impedance upon the layer exposure to an electrolyte solution. In time, water fills the accessible open pores and, in turn, the overall dielectric constant increases, as followed by EIS, until reaching a saturation state (This holds if no corrosion or degradation processes are occurring at the layer−substrate interface. Delamination of the layer from the substrate, clogging of the pores due to accumulation of corrosion products, dissolution of the layer in the solution, all bring a variation of the electrical properties of the layer and have to be taken into account in the EIS investigation.[64]).[25] In order to correlate the variation of the electrical properties with the amount of absorbed water (so-called water uptake), the Brasher−Kingsbury equation is generally adopted.[26] In parallel with the calculation of the diffusivity and water uptake, EIS allows the determination of the open and/or through porosity in a layer. The open porosity of a film deposited on a substrate can be defined as the ratio of the volume of pores with access to the surface (i.e., open-pores) to the volume occupied by the film, while in the through-porosity only pores connected to both the surface and substrate (so-called through-pores) are considered. By means of EIS, the through-porosity can be measured as the ratio, with respect to the pristine substrate, of the charge transfer resistance,[27,28] i.e., the resistance opposed by the layer to charge transfer mechanisms at the substrate surface. This parameter is correlated with the surface area exposed to the surrounding environment and, hence, to the through-porosity. In the literature, porosity values have been measured for inorganic layers, such as SiO_2, Al_2O_3, Ta_2O_5, and TiN.[29−32] Härkönen et al. reported values down to 0.02% for ultrathin ALD deposited Al_2O_3 layers,[28] confirmed by the porosity calculated by means of linear scan voltammetry measurements. Tato et al. detected porosity values down to 0.08% for thick sputtered TiN layers[27] and compared them with the porosity values calculated with both dc and polarization methods.

EIS has also proven to be very sensitive in detecting differences in porosity down to the sub-nanometer regime.[33] Different carbon foams[34] and carbide derived carbon materials[35] have been first characterized by N_2 porosimetry and showed a highly nanoporous structure (average pore size below 1 nm). These materials, exposed to electrolyte solutions, have been studied by impedance spectroscopy. Changes in the impedance spectra among the layers have been attributed to the differences in nanoporosity content and used to categorize the layers with respect to their nanoporosity.

In a solid state configuration, EIS has also been applied for the detection of water vapor in moisture sensors[36−38] and resulted in commercially available devices.[39] An exhaustive and recent review on the subject can be found in ref 40.

In this contribution, we introduce EIS as a characterization tool in the field of moisture barriers. Here, EIS is adopted to categorize the *intrinsic* barrier properties of nanoporous plasma enhanced−chemical vapor deposited (PE-CVD) SiO_2 layers, and the results obtained are complemented by the optochemical properties of the layer measured by spectroscopic ellipsometry (SE), FT-IR, and X-ray photoelectron spectroscopy (XPS). Furthermore, EP is used to determine the relative nanoporosity.

In addition, by measuring the evolution of the layer impedance with EIS following the exposure to an electrolyte solution, the water uptake is determined and found to be in agreement with the open nanoporosity content as determined by means of EP. To corroborate this result, the value of the exponent of the constant phase element used to model the barrier layer by means of EIS was found to linearly correlate with the porosity/optical properties of the layers measured by EP and SE, allowing the determination of the layer nanoporosity. Then, the kinetics of permeation is studied, leading to the determination of the layer diffusion coefficients. Finally, EIS is shown to be sensitive to the presence of local macroscale defects in a barrier layer at a level sufficient to cause its failure during the calcium test (Ca test) measurements. In contrast, EP

DOI: 10.1021/acsami.5b04060
ACS Appl. Mater. Interfaces 2015, 7, 15968−15977

Table 1. Optical, Electrical, and Microstructural Properties for the Layer Investigated, Including *in-Situ* and *Ex-Situ* Refractive Index (n) Measured by SE, Porosity Measured by EP, EC Characteristics, Water Uptake, and Diffusivity Coefficient Measured by EIS

Plasma Power [W]	$n_{in\ situ}$ (±0.003)	$n_{ex\text{-}situ}$ (±0.003)	Porosity (±0.02%)	R_{pore} [Ω cm]	C_{layer} [nF/cm^2]	α (±0.02)	Water Uptake, φ (±0.3%)	Diffusivity, D [cm^2 s^{-1}]
50	1.399	1.447	4.43%	50 ± 3	270 ± 14	0.72	4.2%	$(1.1 \pm 0.1)\cdot10^{-13}$
80	1.403	1.447	3.59%	59 ± 3	215 ± 11	0.77	3.9%	$(2.0 \pm 0.1)\cdot10^{-14}$
110	1.418	1.454	2.61%	2653 ± 13	181 ± 9	0.83	2.9%	$(1.7 \pm 0.1)\cdot10^{-15}$
250	1.457	1.463	0.72%	$(2.5 \pm 0.1) \times 10^5$	45 ± 2	0.98	0.8%	$(9.9 \pm 0.1)\cdot10^{-17}$

and both *ex-situ* and *in situ* SE were found sensitive only to the nanoporosity of the layer, demonstrating the higher sensitivity of EIS with respect to ellipsometric-based techniques in order to evaluate the quality/performance of layers as moisture barriers.

2. MATERIAL AND METHODS

2.1. SiO_2 deposition. SiO_2 layers were deposited on double sided polished n-doped Si wafer (ρ = 1−5 Ω·cm) using a home-built capacitively coupled PE-CVD reactor.[41] Two organosilicon monomers were alternatively adopted, 1,3,5-trivinyl-1,3,5-trimethyl cyclotrisiloxane (V_3D_3, >95%, Gelest) and 1,1,3,5,5-pentamethyl-1,3,5-trivinyltrisiloxane (TVTSO, purity >95%, Gelest). Both were vaporized in a stainless steel bubbler and set at a temperature of 100 °C. The flow-rate was controlled by a vapor source controller (VSC1150C, MKS) and kept constant at 0.5 sccm. The Ar and O_2 flow rates were 70 and 35 sccm, respectively. The pressure was kept constant at 0.3 mbar and the substrate temperature was set at 100 °C. The different porosity content was obtained by depositing the layers at different plasma power density values, in this case with power values in the range 50−250 W (Table 1). The thickness of the layers was measured to be 85 ± 5 nm.

2.2. Electrochemical measurements. Electrochemical Impedance Spectroscopy (EIS) measurements were performed with a potentiostat−galvanostat Autolab-PGSTAT30 and frequency response analyzer (FRA) together with a Faraday cage to avoid external interferences. A three-electrode setup was employed using Ag/AgCl, KCl (sat) as the reference electrode, a graphite rod was used as counter electrode, and the n-type Si substrate served as the working electrode. Good ohmic contact on Si was ensured by back metallization of the wafer with 10 nm of Ti followed by 30 nm of Au, deposited by magnetron sputtering (AJA ATC 1500-F). The area exposed to the electrolyte was 1 cm^2. All tests were performed under ambient temperature in quiescent 0.6 M NaCl electrolyte solution open to air in the frequency range 10^{-1}−10^5 Hz at 10 points/frequency decade. For this, a 10 mV (rms) sine-wave amplitude was applied over the flat band potential (V_{fb}) of the n-type Si substrate to avoid the formation of a space charge capacitance. In order to calculate the V_{fb} a Mott−Schottky analysis[42−44] was employed. For this, the pristine Si substrate was exposed to the electrolyte and the impedance was measured applying bias potentials between 0 and −1 V (vs Ag/AgCl). The V_{fb} was calculated according to the Mott−Schottky relationship:

$$1/C_{sc}^2 = \left(\frac{2}{\varepsilon_0 \varepsilon e N_D}\right)\cdot(V - V_{fb} - k_b T/e) \quad (1)$$

where C_{sc} stands for the surface charge capacitance, ε is the relative permittivity of the semiconductor, and V is the semiconductor electrode potential. The V_{fb} was found to be −0.53 V for n-doped Si in contact with 0.6 M NaCl solution.

The EIS results of the SiO_2 layers were fitted with equivalent electrical circuits (ECs) using Nova software (Metrohm Autolab B.V.) following a procedure previously reported for organic coatings.[45] The goodness of the fit given by chi-square (χ^2) was below 10^{-3} in all cases. From the fitting procedure, the EC characteristic parameters were obtained and the water uptake (φ) and diffusion coefficient (D) calculated as exposed here below.

By considering the barrier layer as a parallel plate capacitor the coating capacitance C is related to the dielectric constant ε by

$$C_{layer} = \frac{\varepsilon \varepsilon_0 A}{d} \quad (2)$$

where ε_0 is the dielectric constant of free space (8.854×10^{-14} F cm^{-1}), A is the surface area of the layer and d is the layer thickness. Since the dielectric constant of SiO_2 is typically in the range 1.9−2.1 and the one of deionized water is 78.4 at 25 °C,[46] the uptake of water leads to an increase in the dielectric constant of the film, and therefore in its capacitance.

The increase in the layer capacitance is related to the volume fraction of water using the Brasher−Kingsbury equation:[26]

$$\varphi = \frac{\log(C_{layer}/C_0)}{\log \varepsilon_w} \quad (3)$$

where C_0 is the capacitance of the dry film extrapolated for t = 0, and ε_w is the dielectric constant of water. φ values can give an indication of the extent of porosity accessible to water molecules. To ensure the validity of this correlation, swelling in the coating should not occur, and the amount of water absorbed should be relatively small and homogeneously permeating in the layer,[26] whereas more complex correlations have to be used to obtain the swelling coefficients.[47−49] Considering the water diffusion to be Fickian (The diffusion is considered Fickian because the mean free path in liquid water (0.25 nm) is smaller than the pore diameter here considered.[65]), φ can be analytically expressed as a function of time,[50] and the diffusivity of the layers calculated by

$$\frac{\log(C_{layer}/C_0)}{\log(C_s/C_0)} = \left[\frac{4D}{d^2\pi}\right]^{1/2} t^{1/2} \quad (4)$$

where C_s is the capacitance at the saturation point, D is the diffusion coefficient, d is the layer thickness, and t is the immersion time. Typically, to reach the saturation stage, the EIS measurements take between few hours and 2−3 days, conditional upon the quality of the barrier layer.

2.3. Opto-chemical characterization. The optical properties of the layers were determined by means of *in situ* and *ex-situ* spectroscopic ellipsometry (SE). *In-situ* SE measurements

DOI: 10.1021/acsami.5b04060
ACS Appl. Mater. Interfaces 2015, 7, 15968−15977

were performed at an angle of incidence of 71.5°, during and at the end of the deposition process, using a J.A. Woollam Co. M-2000F ellipsometer. *Ex-situ* measurements were performed after exposure to air at three angles of incidence (65°, 70°, 75°) in a wavelength range of 190−1000 nm by means of a J.A. Woollam Co. M-2000D ellipsometer.

The chemical characterization of the layers was performed by means of FT-IR spectroscopy and XPS. FT-IR measurements were performed with a Bruker Tensor 27 spectrophotometer in the range 375−4000 cm^{-1} with a resolution of 4 cm^{-1} and 256 scans. Before the spectra acquisition, the spectrometer was purged with N_2 to minimize H_2O and CO_2 absorption. All the reported FT-IR spectra are baseline corrected and normalized with respect to the layer thickness.

XPS was performed using a Thermo Scientific K-Alpha spectrometer with a monochromatic Al Kα X-ray source ($h\nu$ = 1486.6 eV). Prior to the measurements, the samples were presputtered with an Ar ion-gun at an angle of 60° and 1000 eV in order to remove the carbon contamination from the layer surface.

2.4. Porosity characterization by means of ellipsometric porosimetry. The relative amount of open porosity in the layers was determined by means of EP. As previously mentioned, EP is based on the adsorption of a probing molecule in the layer porosity as well as on its surface, leading to a change in the optical properties of the layer. The variation of the refractive index (n) and the possible development of an adsorbate multilayer are followed by SE.

The layers were modeled using a Cauchy function, with the layers being transparent in the spectral range investigated. The probe molecule multilayer uptake was fitted by adding a Cauchy layer on top of the SiO_2 layer with fixed refractive index of the adsorptive, and with its thickness being the only fitting parameter. More details on the modeling can be found in refs 15 and 51.

From the Lorentz−Lorenz relationship, the relative adsorptive volume in pores, with respect to the film volume, can be calculated as

$$V_{ads}/V_{film} = V_{mol}/[\alpha_{ads}\cdot(d_t + d_0)]\cdot((B_S d_0 + B_t d_t) - B_0 d_0) \quad (5)$$

where V_{ads} is the volume of the liquid adsorptive in the pores, V_{film} the volume of the film, B_0 and B_s are the volume polarizability of the film before and during adsorption, B_t is the volume polarizability of the adsorbate multilayer which develops on top of the layer, d_0 and d_t are the thickness of the layer and adsorbate multilayer, respectively, V_{mol} is the molecular volume of the adsorptive, and α_{ads} is the polarizability of the adsorptive molecule.

The adsorptive volume is generally reported as a function of the ratio between the partial pressure (P_l) and the vapor pressure (P_{sat}) of the probe molecule, resulting in a classical adsorption/desorption isotherm. At low P_l/P_{sat} values, the open pores accessible to the adsorptive are filled (micropore filling region), leading to a change in the n values until a monolayer of adsorbate is formed. Afterward, a multilayer of adsorbate develops, detected as a change in the layer thickness. Generally, adsorption isotherms are categorized according to the IUPAC classification.[15,52,53] A type I isotherm is associated with porous materials with a narrow distribution of pore size with a diameter <2 nm (nanoporous or microporous materials), and a type II isotherm is associated with nonporous materials. Mesoporous materials are instead characterized by a type IV isotherm, in which a hysteresis arises in the desorption step, due to the condensation of the adsorbate in the pores.[53,54]

The porosity (P) in the nanoporous regime is calculated, from the isotherm, after the formation of the probe monolayer, i.e., when all the nanopores accessible to the probe molecule are filled. Using the Lorentz−Lorenz equation, P can be expressed as

$$P = \left[\frac{({n_{fill}}^2 - 1)}{({n_{fill}}^2 + 2)} - \frac{({n_0}^2 - 1)}{({n_0}^2 + 2)}\right] \Big/ \frac{({n_{vapor}}^2 - 1)}{({n_{vapor}}^2 + 2)} \quad (6)$$

in which n_0 and n_{fill} are the refractive index values of the layer when the pores are either empty or filled, respectively, and n_{vapor} is the refractive index of the probe molecule. With this approach, the porosity values obtained are independent of the refractive index of the matrix.[15,51]

The home-built porosimeter consisted of a vacuum chamber, equipped with a spectroscopic ellipsometer, Ar is used as carrier gas, and a source of water (d = 0.27 nm) is used as adsorptive. The SE measurements were carried out at an angle of 70°. After loading the SiO_2 sample, the chamber was evacuated overnight in order to remove the adsorbed water due to the layer exposure to ambient. The refractive index value of the SiO_2 layer after evacuation is taken as the starting point for the adsorption measurements (*i.e.*, n_0). Then, the water and Ar are injected into the chamber, and the ratio is adjusted by equilibrium steps in order to scan the entire P_l/P_{sat} range, from 0 to 1.

2.5. Water vapor transmission rate (WVTR) measurements: calcium test (Ca test). Water vapor transmission rate (WVTR) measurements are carried out by means of the Ca test according to the procedure described by Nisato et al.,[55,56] at a constant temperature of 20 °C and a relative humidity (R.H.) of 50%. For this test, the measured barrier layer is stacked with a 40-nm-thick Ca layer. Upon exposure to moisture, any changes to the optical transmittance of the Ca layer can be attributed to oxidation of the Ca to CaO and, hence, to permeation of water vapor through the barrier layer. To obtain results with 10% precision, the test should last until at least 1 nm of the Ca material has been oxidized, and in the experimental condition chosen, a single measurement takes between a few weeks to several months, depending on the goodness of the tested barrier. The *intrinsic* WVTR is measured by excluding the local white spots from the measurement which develop due to localized fast oxidation of Ca and are associated with the water permeating through a macrodefect or pinhole. In this way, only the permeation through nanopores is considered.

The measurement setup for the Ca test (developed by the Philips Research laboratories) consists of a Philips CL5000 M light source with a diffuser for uniform back lighting and a sample holder with mask. A 12 bit Adimex MX12p camera was used to obtain a gray scale image of the sample. The extent of oxidation is determined from the gray scale. More details about the setup can be found elsewhere.[16] Ca is deposited on glass substrates, followed by the deposition of the a temporary PE-CVD SiO_x (*intrinsic* WVTR of 10^{-2} g m^{-2} day^{-1}) barrier layer, to avoid oxidation during transportation. The use of the temporary SiO_x layer has no effect on the determined *intrinsic* WVTR values, since its barrier performance is 1-to-3 orders of magnitude lower than the barrier layers under investigation. The barrier layer is deposited last, on top of the SiO_x layer. The final configuration is glass/Ca/40 nm-SiO_x/barrier layer.

DOI: 10.1021/acsami.5b04060
ACS Appl. Mater. Interfaces 2015, 7, 15968−15977

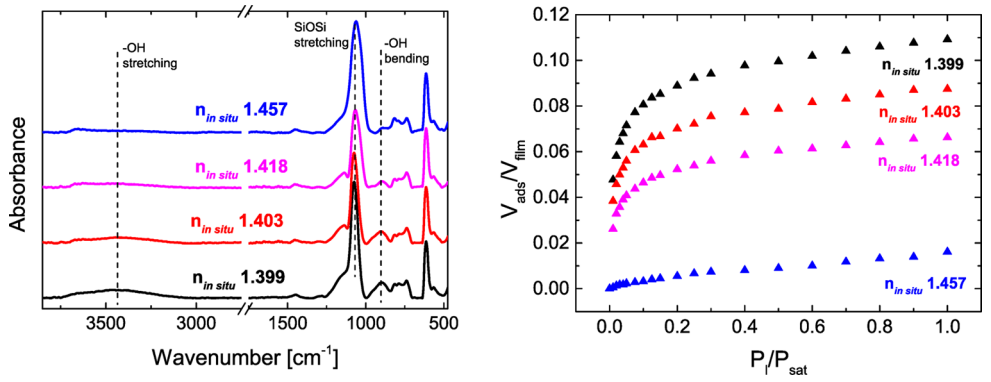

Figure 1. (a) FT-IR analysis of the PE-CVD SiO_2 layers. The *in situ* refractive index is also reported. (b) EP isotherms for the PE-CVD SiO_2 layers deposited by means of V_3D_3. Water is used as probe molecule. The data are reported as V_{ads}/V_{film} vs water partial pressure (P_l/P_{sat}).

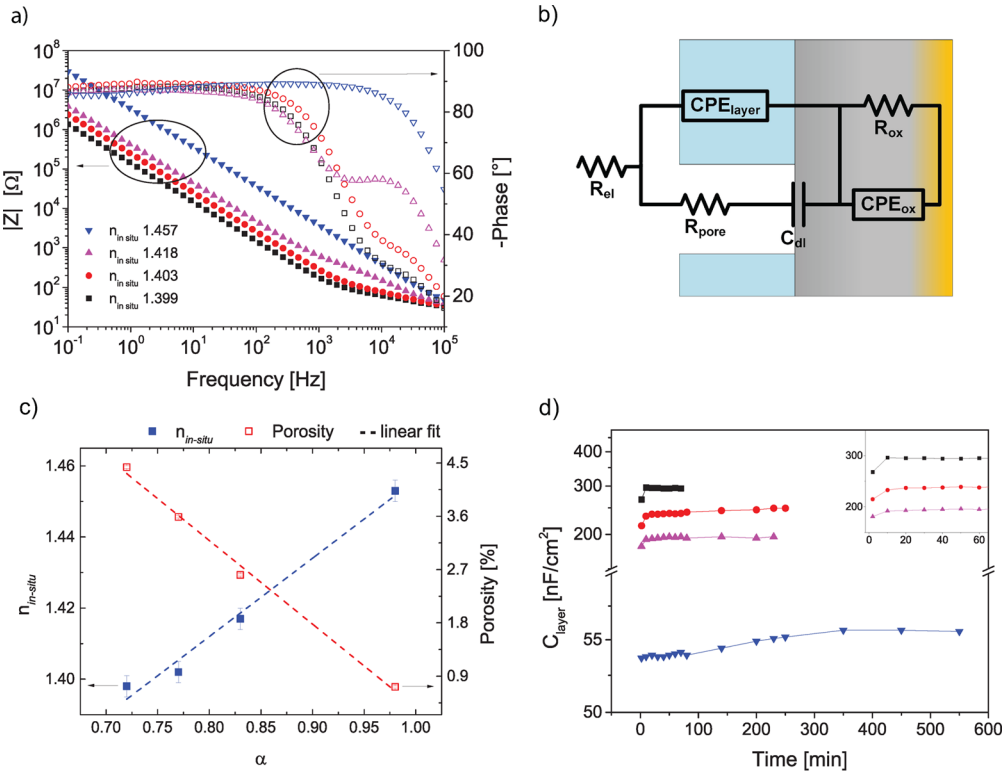

Figure 2. (a) Bode plots of PE-CVD SiO_2 layers after 2 min of immersion in a 0.6 M NaCl solution: impedance module and phase vs frequency. (b) EC used to model the impedance data. (c) *in situ* refractive index ($n_{in\ situ}$) as measured by SE, and porosity as measured by EP as a function of the α fitting value of the CPE. (d) Variation of the C_{layer} vs immersion time for all the PE-CVD SiO_2 layers. In the inset: zoom on the first hour of immersion for the C_{layer} of $SiO_{2,n1.399}$, $SiO_{2,n1.403}$, $SiO_{2,n1.418}$.

3. RESULTS AND DISCUSSION

3.1. Opto-chemical characterization. In order to get information on the degree of cross-linking reached in the deposited silicon dioxide layers, FTIR studies were performed (Figure 1a). The FT-IR measurements showed silanol (SiOH)-related absorption stretching and bending bands in all the films (Figure 1a). This indicates the presence of a range of porosity as a function of the deposition power, since the Si−OH groups are chain-terminating groups[57] leading to free volume.

The *in situ* refractive index ($n_{in\ situ}$) values confirm the IR analysis: the values are below the refractive index of fused silica (1.465 at 633 nm),[14] confirming the presence of porosity in the layers (see Table 1 and Figure 1a). This result is further supported by the aging (Δn) of the samples resulting from their exposure to the environment and measured by *ex-situ* SE (Table 1). As expected, it is found that the refractive index increases due to moisture uptake, and that this effect is more pronounced for layers with lower *n* values. In a previous work, we have shown for oxide layers that a correlation exists between the *in situ* refractive index values, porosity, and *intrinsic* barrier properties.[15] Based on this work the barrier performance of the layers can be predicted depending on the $n_{in\ situ}$ values. Using this approach the *i*-WVTR values were found to range from 10^{-2} gm^{-2} day^{-1} for the highly porous $SiO_{2,n1.399}$ to 10^{-5} gm^{-2} day^{-1} for the low-porous $SiO_{2,n1.457}$.

The XPS measurements pointed out the absence of carbon originating from the precursor chemical structure and a O/Si ratio of 2.1 ± 0.1 for all layers. The lack of carbon prevents potential swelling effects during the EIS measurement in electrolyte solution, assuring the applicability of the Brasher−

DOI: 10.1021/acsami.5b04060
ACS Appl. Mater. Interfaces 2015, 7, 15968−15977

Kingsbury equation.[58] This is confirmed by *ex-situ* SE measurements performed on the samples after exposure to the electrolyte solution, which showed no increase in thickness.

3.2. Microstructural characterization. In order to identify the nature of the open porosity and determine the relative amount of pores accessible to water molecules, the microstructure of the PE-CVD SiO_2 layers was characterized by EP using water (d = 0.27 nm) as adsorptive. The layers and the adsorption were modeled with a Cauchy function as described in the Material and Methods. In the literature, a Bruggerman effective media approximation (B-EMA) function is often used to model porous systems.[59,60] However, in order to use this approach, the optical constants of the layer matrix must be known, and these are often obtained by studying nonporous reference samples.[61] For the PE-CVD SiO_2 layers under investigation, the matrix optical constants cannot be measured directly, being different from a pure silica layer, and they can be otherwise extrapolated by empirical methods.[62] On the contrary, the Cauchy function adopted in this study avoids making assumptions on the layer optical constants, and the system is hence represented by a homogeneous combination of voids and layer matrix. In Figure 1b, the adsorption isotherms expressed as adsorbed water volume as a function of the P_l/P_{sat} are reported. All layers showed a type I isotherm. Such a result confirms the presence of nanoporous layers with a pore diameter below 2 nm. No mesoporosity was detected, as the desorption did not show hysteresis typical of a type IV isotherm.[53] The open porosity values, calculated according to eq 6, were found to range between 4.2% and 0.7% (Table 1). The differences in porosity pointed out by FT-IR measurements and *in situ* refractive index values are confirmed by the differential uptake in terms of V_{ads} at low P_l/P_{sat}, i.e., in the micropore filling region. The $SiO_{2,n1.457}$ showed a combination of type I and type II isotherms, which is characterized, next to the micropore filling, by a multilayer development.[17] The type I +II is generally assigned to microporous layers with a very low porosity content, which is filled by the adsorptive at P_l/P_{sat} values below 0.1−0.2 and allows the development of a multilayer already at low P_l/P_{sat}.

3.3. EIS measurements. *3.3.1. Nanoporosity detection.* EIS was adopted to follow the change in the SiO_2 layer capacitance upon immersion in the electrolyte solution, until saturation occurred, given when all the pores accessible to the electrolyte solution were filled. The EIS data are reported in this work as impedance modulus (|Z|) and phase angle as a function of the frequency (Bode plots). The Bode plots of the layers at the beginning of the immersion in the electrolyte solution are shown in Figure 2a.

The impedance modulus values at all frequencies confirm the trend of n, Δn, and EP measurements earlier discussed where the highest and lowest |Z| values are shown by $SiO_{2,n1.457}$ and $SiO_{2,n1.399}$, respectively.

The sensitivity of the technique in discerning small differences in porosity was compared with more classical characterization tools for thin films such as SE. The layers showing the highest porosity content with the lowest *in situ* n values ($SiO_{2,n1.399}$ and $SiO_{2,n1.403}$) exhibit the same refractive index when measured *ex-situ* (see Table 1), highlighting a sensitivity limitation of this approach. However, EIS was able to discern between the two layers in terms of |Z| values because of the higher detection limit (on the order of 10^{-2}−10^{-3} Ω), demonstrating a higher sensitivity when compared to *ex-situ* SE. For the layers with $n_{in\ situ}$ in the range 1.399−1.418, the |Z| plots show a two-slope behavior. In the low frequency region, the slope is −0.98 ± 0.02, which is characteristic of a pure capacitor[63] and here attributed to the Si substrate. The capacitive behavior is confirmed by the phase Bode plots, which show a constant value close to 90°. In the high frequency region, the slope varies from −0.32 ± 0.02 ($SiO_{2,n1.399}$) to −0.63 ± 0.02 ($SiO_{2,n1.418}$), and the phase between 28° and 57°. This indicates an increase in the barrier properties of the layers with the refractive index and correlates with the microstructural characterization. The two-slope behavior disappears for the $SiO_{2,n1.457}$ with a constant slope of −0.99 ± 0.02 and a phase value close to 90° in the frequency range 10^4−10^{-1} Hz. Such results confirm the highest capacitive behavior of the system with the highest n, this being associated with a lower porosity reflected in a combined type I+II isotherm.

3.3.2. Equivalent circuit and water permeation. As aforementioned, the water permeation characteristics of inorganic layers offer essential information to categorize their barrier performance. Furthermore, the water uptake values obtained with EIS can give extra information on the extent of porosity in the layer accessible to the water molecules. In order to calculate φ and D values, the impedance data were modeled with the most probable equivalent circuit (MPEC) shown in Figure 2b, obtained after a dedicated selection process.[45] In this MPEC, R_{el} represents the resistance of the electrolyte solution, C_{layer} is the capacitance attributed to the barrier layer, R_{pore} is the pore resistance, C_{dl} is the capacitance that arises for the formation of a double layer at the substrate surface, and C_{ox} and R_{ox} are the capacitance and resistance of the native oxide layer at the substrate surface, respectively. Compared to the classical EC for defective layers,[23] the so-called polarization/charge transfer resistance cannot be used to model the impedance data of these systems due to the inertness of the Si substrate under the chosen experimental conditions that prevents corrosion processes/charge transfer mechanisms from occurring.

In order to improve the fit and due to the presence of inhomogeneity, the layer capacitances of all the SiO_2 layers were substituted with Constant Phase Elements (CPE)[23,32] defined as

$$Z_{CPE,layer} = \frac{1}{Q_{layer}\cdot(i\omega)^{\alpha}} \tag{7}$$

where i is the imaginary number, ω is the radial frequency, Q_{layer} is a constant value, independent of frequency, and α is the CPE power, which gives an indication of the layer inhomogeneity/porosity. In Table 1, the EC fitted parameters of interest for the layers at the beginning of the immersion are presented.

The C_{layer} and R_{pore} values are in agreement with the barrier properties and porosity content inferred by SE (*in situ*, Δn), FT-IR, and EP measurements. As n approaches the value for fused silica, the layer shows a higher capacitive behavior and pore resistance. Furthermore, the α values range from 0.72 to 0.98 for the most and least porous layer, respectively, highlighting the relation of this parameter to the inhomogeneity/nanoporosity of the layer. The increase of the α value points out that the heterogeneity and porosity decrease with the increase in n, giving an indication of the increased barrier properties of the layer. Moreover, it confirms the observations based on the different slopes in the impedance modulus in the Bode plot. When plotting the α value vs both the $n_{in\ situ}$ and the nanoporosity values, a clear linear correlation was found, as shown in Figure 2c. This relationship allows for the

DOI: 10.1021/acsami.5b04060
ACS Appl. Mater. Interfaces 2015, 7, 15968−15977

determination of the nanoporosity values starting from the CPE attributed to the barrier layer, pointing out the goodness of the fit and the sensitivity of EIS toward the detection of the nanoporosity/free volume.

The barriers were further kept in the electrolyte solution, and the permeation of water was followed by monitoring the increase of the layer capacitance values until saturation occurred. In Figure 2d the evolution of the C_{layer} for all the layers as a function of the immersion time is shown. From the variation of the layer capacitance, the water uptake values and diffusivity coefficients were calculated as indicated in the experimental section (Table 1). The water uptake values are in good agreement with the porosity values calculated by EP, confirming the applicability of the Brasher−Kingsbury equation also for thin inorganic layers. The diffusivity coefficients are comparable to those reported in the literature for analogous moisture barriers,[4,22] and they are understandably lower than those of thin corrosion protection organic layers,[43,58] all this supporting the sensitivity of EIS in evaluating moisture barrier layers in a quantitative manner.

3.3.3. Local macroscale defects identification. As previously mentioned, water permeates into a barrier layer through both macroscale defects and nanopores. EP is able to detect and quantify nanoporosity (as well as mesoporosity, if present), but it is limited in the detection of localized larger defects. Instead, in this session, EIS will be shown able to distinguish between the permeation of water through macroscale defects and nanoporosity, detecting macroscale defect levels sufficient to cause the failure of the barrier layer during the Ca test measurements.

In parallel studies on moisture barriers, PE-CVD SiO_2 layers have been deposited with TVTSO. The TVTSO-deposited SiO_2 showed the same composition and refractive index values (both *in situ* and *ex-situ*) compared to the ones deposited by V_3D_3. Both layers were tested with the Ca test in order to determine their *i*-WVTR values. In Figure 3, the Ca oxidation followed in time for a V_3D_3- and TVTSO-deposited PE-CVD SiO_2 layer is presented.

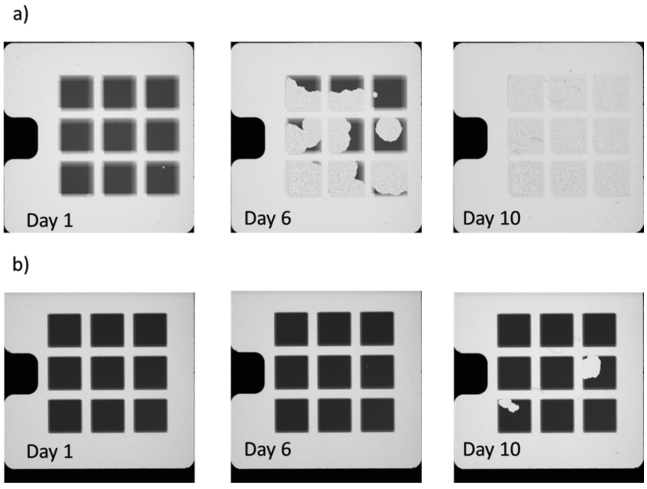

Figure 3. Calcium plates used in the Ca test, after one, six, and 10 days of measurements: (a) TVTSO-deposited PE-CVD $SiO_{2,n1.447}$, showing a pinhole density per plate of 772 after 10 days and a pin area of 4.84 mm^2, and (b) V_3D_3-deposited PE-CVD $SiO_{2,n1.447}$, showing a pinhole density per plate of 2 after 10 days and a pin area of 0.5 mm^2.

The layers showed the same value of refractive index ($n_{in\ situ}$ of 1.447 ± 0.003), and the measured *i*-WVTR value fell in the 10^{-5} gm^{-2} day^{-1} regime, as expected ($(4 \pm 1) \times 10^{-5}$ gm^{-2} day^{-1} and $(3 \pm 3) \times 10^{-5}$ gm^{-2} day^{-1} for the V_3D_3- and TVTSO-deposited layers, respectively).[15] However, as shown in Figure 3a, the TVTSO-deposited layer showed a high density of pinholes (772 pinholes per plate after 10 days) and a pinhole area of 4.54 mm^2, and the Ca plate became completely oxidized after 10 days. On the contrary, the V_3D_3-deposited layer (Figure 3b) showed a pinhole density 2 orders of magnitude lower (2 pinholes per plate after 10 days), and a pinhole area ten times lower (0.55 mm^2).

To further investigate the difference in macroscale defects density, different TVTSO- and V_3D_3-deposited SiO_2 layers were investigated with EP and EIS. In Figure 4, the Bode plots and adsorption isotherms of the V_3D_3-deposited $SiO_{2,n1.418}$ and $SiO_{2,n1.457}$ are reported together with the plots of a TVTSO-deposited layer with an *in situ* refractive index value of 1.446 ($SiO_{2n1.446}$).

In Figure 4a, the EP measurements are reported and point out a type I isotherm for all the layers. The *P* value of the $SiO_{2n1.446}$ was found to be 1.5%, following the trend indicated by the isotherm and inferred by the *in situ* refractive index value. However, the EIS measurement showed a more defective nature of the TVTSO-deposited layers (Figure 4b). In the high frequency region, the Bode plots of the $SiO_{2n1.446}$ showed a similar trend obtained for the V_3D_3-deposited layer, with a phase value close to 90° and a |Z| slope close to −1, in agreement with the low porosity value inferred by EP. Nevertheless, a second time constant developed in the Bode plot for the $SiO_{2n1.446}$, in a frequency range which is generally attributed to the formation of an interface between the substrate and the electrolyte solution,[23,32] while the V_3D_3-deposited layers only showed the contribution of the substrate, as aforementioned. Following the permeation of water in the TVTSO-deposited layer as a function of change of the C_{layer}, the φ and *D* values pointed out a higher water permeation than the V_3D_3-deposited layers, with a water uptake of 6.5% and a diffusivity of 9.4×10^{-15} cm^2 s^{-1} (Table 2). The φ value was found to be higher than the most porous layer investigated in this study ($SiO_{2,n1.399}$), while the *D* coefficient was found close to the one of the $SiO_{2,n1.403}$ layer, both pointing out the higher defective nature of the TVTSO-deposited layer, in agreement with the high macroscale defect density inferred by the Ca test.

The limits of EP in detecting the macroscale defects arise from the defect dimension, ranging between hundreds of nanometers to several micrometers. Due to the large distance of the defect walls, the probe molecule adsorption does not lead to a variation of the refractive index, and it develops instead as multilayer t. On the other hand, EIS was able to detect the presence of defects/pinholes in the layer, a high density of which leads to the fast oxidation of the calcium plate in the Ca test. This result infers the potential use of impedance spectroscopy in the prediction of the failure of a barrier layer in the Ca test due to the permeation through local macrodefects.

4. CONCLUSIONS

EIS was successfully applied to PE-CVD SiO_2 thin layers to categorize them in terms of their encapsulation barrier properties, i.e., pore resistance and capacitance behavior, water uptake, and diffusion coefficient. EIS showed a higher sensitivity than the classical *ex-situ* ellipsometric studies and is

DOI: 10.1021/acsami.5b04060
ACS Appl. Mater. Interfaces 2015, 7, 15968−15977

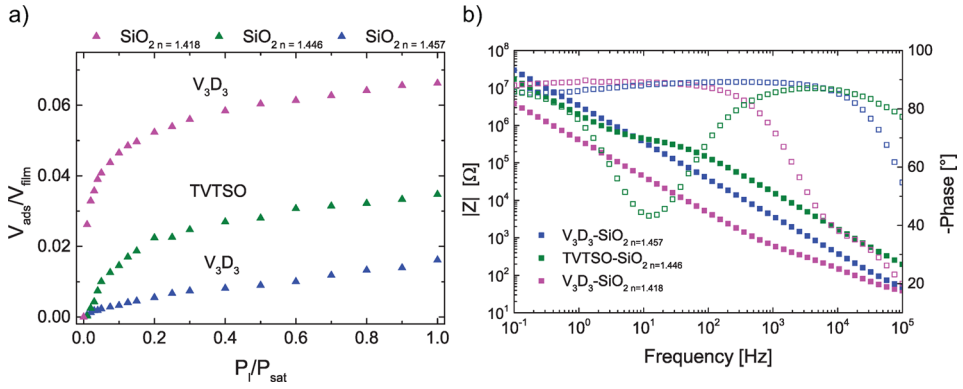

Figure 4. V_3D_3-deposited ($SiO_{2n1.457}$ and $SiO_{2,n1.418}$) compared to TVTSO-deposited SiO_2 ($SiO_{2,n1.446}$): (a) EP adsorption isotherm; (b) Bode plots after 2 min of immersion.

Table 2. V_3D_3-Deposited ($SiO_{2,n1.457}$ and $SiO_{2,n1.418}$) Compared to TVTSO-Deposited SiO_2 ($SiO_{2,n1.446}$): *in-Situ* Refractive Index, Porosity Measured by EP, Water Uptake, and Diffusivity Measured by EIS

Precursor	PE-CVD SiO_2, $n_{in\ situ}$	P by EP (±0.02%)	Water uptake	Diffusivity [$cm^2\ s^{-1}$]
V_3D_3	1.418	2.61	2.9%	$(1.7 \pm 0.1) \times 10^{-15}$
TVTSO	1.446	1.51	6.5%	$(9.4 \pm 0.1) \times 10^{-15}$
V_3D_3	1.457	0.72	0.8%	$(9.9 \pm 0.1) \times 10^{-17}$

suitable for a fast and quantitative characterization of the water barrier performance. Furthermore, the variation of C_{layer}, φ, and D values was calculated for the first time on inorganic layers by means of EIS. Water uptake values down to 0.8% were obtained by applying the Brasher−Kingsbury equation and were found in agreement with the open nanoporosity values measured by ellipsometric porosimetry. Diffusion coefficients as low as $(9.9 \pm 0.1) \times 10^{-17}$ $cm^2\ s^{-1}$ were measured and are in agreement with previous studies on single inorganic moisture permeation barriers. A good linear correlation between the *in situ* refractive indexes (n)/nanoporosity and the exponent α from the CPE used in the fittings of the EIS data was obtained. This suggests the possibility of the direct calculation of open nanoporosity from an EIS fit, although more tests with other materials need to be performed to confirm this result.

Moreover, EIS was found able to detect the presence of levels of pinholes/defects sufficient to cause the failure of the barrier in the Ca test, overcoming the limits of *in situ* SE and ellipsometric porosimetry. TVTSO-deposited SiO_2, categorized as nanoporous by means of EP, showed the presence of a large number of macroscale defects in the EIS spectra, confirmed by the failure of the Ca test measurements due to the fast water permeation through the macroscale permeation pathways. In this work, EIS was demonstrated as a valuable and fast technique in the evaluation of the quality of moisture barrier layers and identification of both nanoporosity and local macroscale defects, complementing the microstructural characterization of optical methods such as spectroscopic ellipsometric porosimetry and calcium test.

AUTHOR INFORMATION

Corresponding Author

*E-mail: a.perrotta@tue.nl. Phone: +31402474095.

Funding

This work forms part of the research program of the Dutch Polymer Institute (DPI) project #752 of the Large Area Thin Film Electronics (LATFE) program..

Notes

The authors declare no competing financial interest.

ACKNOWLEDGMENTS

The authors would like to thank J. J. A. Zeebregts, J. J. L. M. Meulendijks, C. O. van Bommel, and W. Keuning for their skillful technical assistance. T. van Mol, G. Kirchner (Holst Centre, High Tech Campus, Eindhoven, The Netherlands), P. van de Weijer, and P. Klaassen (Philips Research, High Tech Campus, Eindhoven) are kindly acknowledged for the WVTR measurements and the data discussion. M.C. acknowledges the Aspasia NWO program.

REFERENCES

(1) Kim, Y.; Kim, N.; Kim, H.; Graham, S. The Development of Thin Film Barriers for Encapsulating Organic Electronics. In *2011 IEEE 61st Electronic Components and Technology Conference (ECTC)*; IEEE: 2011; pp 2101−2106.

(2) Kim, L. H.; Kim, K.; Park, S.; Jeong, Y. J.; Kim, H.; Chung, D. S.; Kim, S. H.; Park, C. E. Al2O3/TiO2 Nanolaminate Thin Film Encapsulation for Organic Thin Film Transistors via Plasma-Enhanced Atomic Layer Deposition. *ACS Appl. Mater. Interfaces* **2014**, *6* (9), 6731−6738.

(3) Tropsha, Y. G.; Harvey, N. G. Activated Rate Theory Treatment of Oxygen and Water Transport through Silicon Oxide/Poly(ethylene terephthalate) Composite Barrier Structures. *J. Phys. Chem. B* **1997**, *101* (13), 2259−2266.

(4) Graff, G. L.; Williford, R. E.; Burrows, P. E. Mechanisms of Vapor Permeation Through Multilayer Barrier Films: Lag Time versus Equilibrium Permeation. *J. Appl. Phys.* **2004**, *96* (4), 1840−1849.

(5) Seo, S.-W.; Jung, E.; Lim, C.; Chae, H.; Cho, S. M. Water Permeation through Organic−Inorganic Multilayer Thin Films. *Thin Solid Films* **2012**, *520* (21), 6690−6694.

(6) Fahlteich, J.; Fahland, M.; Schönberger, W.; Schiller, N. Permeation Barrier Properties of Thin Oxide Films on Flexible Polymer Substrates. *Thin Solid Films* **2009**, *517* (10), 3075−3080.

(7) Lewis, J. Material Challenge for Flexible Organic Devices. *Mater. Today* **2006**, *9* (4), 38−45.

(8) Spee, D. A.; Rath, J. K.; Schropp, R. E. I. Using Hot Wire and Initiated Chemical Vapor Deposition for Gas Barrier Thin Film Encapsulation. *Thin Solid Films* **2015**, *575*, 67−71.

(9) Stevens, M.; Tuomela, S.; Mayer, D. Water Vapor Permeation Testing of Ultra-Barriers: Limitations of Current Methods and Advancements Resulting in Increased Sensitivity. In *Society of Vacuum*

DOI: 10.1021/acsami.5b04060
ACS Appl. Mater. Interfaces 2015, 7, 15968−15977

Coaters 48 th Annual Technical Conference Proceedings; 2005; pp 189−191.
(10) Higgs, D.; Young, M.; Bertrand, J. A.; George, S. M. Oxidation Kinetics of Calcium Films by Water Vapor and Their Effect on Water Vapor Transmission Rate Measurements. *J. Phys. Chem. C* **2014**, *118* (50), 29322−29332.
(11) Roberts, A. P.; Henry, B. M.; Sutton, A. P.; Grovenor, C. R. M.; Briggs, G. A. D.; Miyamoto, T.; Kano, M.; Tsukahara, Y.; Yanaka, M. Gas Permeation in Silicon-Oxide/Polymer (SiOx/PET) Barrier Films: Role of the Oxide Lattice, Nano-Defects and Macro-Defects. *J. Membr. Sci.* **2002**, *208* (1−2), 75−88.
(12) Affinito, J.; Hilliard, D. A New Class of Ultra-Barrier Materials. In *Society of Vacuum Coaters 47th Annual Technical Conference Proceedings*; 2004; pp 563−593.
(13) Da Silva Sobrinho, A. S.; Czeremuszkin, G.; Latrèche, M.; Wertheimer, M. R. Defect-Permeation Correlation for Ultrathin Transparent Barrier Coatings on Polymers. *J. Vac. Sci. Technol., A* **2000**, *18* (1), 149−157.
(14) Erlat, A. G.; Wang, B.-C.; Spontak, R. J.; Tropsha, Y.; Mar, K. D.; Montgomery, D. B.; Vogler, E. A. Morphology and Gas Barrier Properties of Thin SiOx Coatings on Polycarbonate: Correlations with Plasma-Enhanced Chemical Vapor Deposition Conditions. *J. Mater. Res.* **2000**, *15* (03), 704−717.
(15) Perrotta, A.; van Beekum, E. R. J.; Aresta, G.; Jagia, A.; Keuning, W.; van de Sanden, M. C. M.; Kessels, W. M. M.; Creatore, M. On the Role of Nanoporosity in Controlling the Performance of Moisture Permeation Barrier Layers. *Microporous Mesoporous Mater.* **2014**, *188*, 163−171.
(16) Keuning, W.; van de Weijer, P.; Lifka, H.; Kessels, W. M. M.; Creatore, M. Cathode Encapsulation of Organic Light Emitting Diodes by Atomic Layer Deposited Al2O3 Films and Al2O3/A-SiNx:H Stacks. *J. Vac. Sci. Technol., A* **2012**, *30* (1), 01A131.
(17) Baklanov, M. R.; Mogilnikov, K. P.; Polovinkin, V. G.; Dultsev, F. N. Determination of Pore Size Distribution in Thin Films By Ellipsometric Porosimetry. *J. Vac. Sci. Technol., B: Microelectron. Process. Phenom.* **2000**, *18* (3), 1385−1391.
(18) Bourgeois, A.; Brunet-Bruneau, A.; Fisson, S.; Demarets, B.; Grosso, D.; Cagnol, F.; Sanchez, C.; Rivory, J. Determination of Pore Size Distribution in Thin Organized Mesoporous Silica Films by Spectroscopic Ellipsometry in the Visible and Infrared Range. *Thin Solid Films* **2004**, *447−448*, 46−50.
(19) Sree, S. P.; Dendooven, J.; Smeets, D.; Deduytsche, D.; Aerts, A.; Vanstreels, K.; Baklanov, M. R.; Seo, J. W.; Temst, K.; Vantomme, A.; Detavernier, C.; Martens, J. A. Spacious and Mechanically Flexible Mesoporous Silica Thin Film Composed of an Open Network of Interlinked Nanoslabs. *J. Mater. Chem.* **2011**, *21* (21), 7692−7699.
(20) Grill, A.; Patel, V.; Rodbell, K. P.; Huang, E.; Baklanov, M. R.; Mogilnikov, K. P.; Toney, M.; Kim, H.-C. Porosity in Plasma Enhanced Chemical Vapor Deposited SiCOH Dielectrics: a Comparative Study. *J. Appl. Phys.* **2003**, *94* (5), 3427−3435.
(21) Fuertes, M. C.; Colodrero, S.; Lozano, G.; González-Elipe, A. R.; Grosso, D.; Boissière, C.; Sánchez, C.; Soler-Illia, G. J. D. A. A.; Míguez, H. Sorption Properties of Mesoporous Multilayer Thin Films. *J. Phys. Chem. C* **2008**, *112*, 3157−3163.
(22) Carcia, P. F.; McLean, R. S.; Reilly, M. H.; Groner, M. D.; George, S. M. Ca Test of Al2O3 Gas Diffusion Barriers Grown by Atomic Layer Deposition on Polymers. *Appl. Phys. Lett.* **2006**, *89* (3), 031915.
(23) Amirudin, A.; Thieny, D. Application of Electrochemical Impedance Spectroscopy to Study the Degradation of Polymer-Coated Metals. *Prog. Org. Coat.* **1995**, *26* (1), 1−28.
(24) Barranco, V.; Thiemann, P.; Yasuda, H. K.; Stratmann, M.; Grundmeier, G. Spectroscopic and Electrochemical Characterisation of Thin Cathodic Plasma Polymer Films on Iron. *Appl. Surf. Sci.* **2004**, *229* (1−4), 87−96.
(25) Mansfeld, F. Use of Electrochemical Impedance Spectroscopy for the Study of Corrosion Protection by Polymer Coatings. *J. Appl. Electrochem.* **1995**, *25* (3), 187−202.
(26) Brasher, D. M.; Kingsbury, A. H. Electrical Measurements in the Study of Immersed Paint Coatings on Metal. I. Comparison between Capacitance and Gravimetric Methods of Estimating Water-Uptake. *J. Appl. Chem.* **1954**, *4* (2), 62−72.
(27) Tato, W.; Landolt, D. Electrochemical Determination of the Porosity of Single and Duplex PVD Coatings of Titanium and Titanium Nitride on Brass. *J. Electrochem. Soc.* **1998**, *145*, 4173−4181.
(28) Härkönen, E.; Díaz, B.; Światowska, J.; Maurice, V.; Seyeux, A.; Vehkamäki, M.; Sajavaara, T.; Fenker, M.; Marcus, P.; Ritala, M. Corrosion Protection of Steel with Oxide Nanolaminates Grown by Atomic Layer Deposition. *J. Electrochem. Soc.* **2011**, *158* (11), C369−C378.
(29) Ahn, S. H.; Lee, J. H.; Kim, H. G.; Kim, J. G. A Study on the Quantitative Determination of Through-coating Porosity in PVD-grown Coatings. *Appl. Surf. Sci.* **2004**, *233* (1−4), 105−114.
(30) Díaz, B.; Światowska, J.; Maurice, V.; Seyeux, A.; Normand, B.; Härkönen, E.; Ritala, M.; Marcus, P. Electrochemical and Time-of-Flight Secondary Ion Mass Spectrometry Analysis of Ultra-Thin Metal Oxide (Al2O3 and Ta2O5) Coatings Deposited by Atomic Layer Deposition on Stainless Steel. *Electrochim. Acta* **2011**, *56* (28), 10516−10523.
(31) Díaz, B.; Härkönen, E.; Światowska, J.; Maurice, V.; Seyeux, A.; Marcus, P.; Ritala, M. Low-Temperature Atomic Layer Deposition of Al2O3 Thin Coatings for Corrosion Protection of Steel: Surface and Electrochemical Analysis. *Corros. Sci.* **2011**, *53* (6), 2168−2175.
(32) Sidi Ali Cherif, K.; Kordic, S.; Farkas, J.; Szunerits, S. Electrochemical Impedance Spectroscopy of Dense Silica and Porous Silicon Oxycarbide. *Electrochem. Solid-State Lett.* **2007**, *10* (9), G63−G67.
(33) Kant, K.; Priest, C.; Shapter, J. G.; Losic, D. The Influence of Nanopore Dimensions on the Electrochemical Properties of Nanopore Arrays Studied by Impedance Spectroscopy. *Sensors* **2014**, *14* (11), 21316−21328.
(34) Kalluri, R. K.; Biener, M. M.; Suss, M. E.; Merrill, M. D.; Stadermann, M.; Santiago, J. G.; Baumann, T. F.; Biener, J.; Striolo, A. Unraveling the Potential and Pore-Size Dependent Capacitance of Slit-Shaped Graphitic Carbon Pores in Aqueous Electrolytes. *Phys. Chem. Chem. Phys.* **2013**, *15* (7), 2309−2320.
(35) Largeot, C.; Portet, C.; Chmiola, J.; Taberna, P.; Gogotsi, Y.; Simon, P. Relation between the Ion Size and Pore Size for an Electric Double-Layer Capacitor. *J. Am. Chem. Soc.* **2008**, *130* (9), 2730−2731.
(36) Feng, Z.; Chen, X.-J.; Chen, J.; Hu, J. A Novel Humidity Sensor Based on Alumina Nanowire Films. *J. Phys. D: Appl. Phys.* **2012**, *45*, 225305.
(37) Almasi Kashi, M.; Ramazani, A.; Abbasian, H.; Khayyatian, A. Capacitive Humidity Sensors Based on Large Diameter Porous Alumina Prepared by High Current Anodization. *Sens. Actuators, A* **2012**, *174*, 69−74.
(38) Faia, P. M.; Furtado, C. S.; Ferreira, A. J. AC Impedance Spectroscopy: a New Equivalent Circuit for Titania Thick Film Humidity Sensors. *Sens. Actuators, B* **2005**, *107* (1), 353−359.
(39) Chakraborty, S.; Nemoto, K.; Hara, K.; Lai, P. T. Moisture Sensitive Field Effect Transistors Using Gate Structure. *Smart Mater. Struct.* **1999**, *8* (2), 274−277.
(40) Farahani, H.; Wagiran, R.; Hamidon, M. N. Humidity Sensors Principle, Mechanism, and Fabrication Technologies: a Comprehensive Review. *Sensors* **2014**, *14* (5), 7881−7939.
(41) Aresta, G.; Palmans, J.; van de Sanden, M. C. M.; Creatore, M. Initiated-Chemical Vapor Deposition of Organosilicon Layers: Monomer Adsorption, Bulk Growth, and Process Window Definition. *J. Vac. Sci. Technol., A* **2012**, *30* (4), 041503.
(42) Gomes, W. P.; Vanmaekelbergh, D. Impedance Spectroscopy at Semiconductor Electrodes: Review and Recent Developments. *Electrochim. Acta* **1996**, *41* (7−8), 967−973.
(43) Vlasak, R.; Klueppel, I.; Grundmeier, G. Combined EIS and FTIR−ATR Study of Water Uptake and Diffusion in Polymer Films on Semiconducting Electrodes. *Electrochim. Acta* **2007**, *52* (28), 8075−8080.

DOI: 10.1021/acsami.5b04060
ACS Appl. Mater. Interfaces 2015, 7, 15968−15977

(44) Hens, Z.; Gomes, W. P. Electrochemical Impedance Spectroscopy at Semiconductor Electrodes: the Recombination Resistance Revisited. *J. Electroanal. Chem.* **1997**, *437* (1−2), 77−83.
(45) Garcia, S. J.; Markley, T. A.; Mol, J. M. C.; Hughes, A. E. Unravelling the Corrosion Inhibition Mechanisms of Bi-functional Inhibitors by EIS and SEM−EDS. *Corros. Sci.* **2013**, *69*, 346−358.
(46) Murrel, J. N.; Jenkins, A. D. *Properties of Liquids and Solutions*, 2nd ed.; Wiley: 1994.
(47) Calderón-Gutierrez, J. A.; Bedoya-Lora, F. E. Barrier Property Determination and Lifetime Prediction by Electrochemical Impedance Spectroscopy of a High Performance Organic Coating. *Dyna* **2014**, *81* (183), 97−106.
(48) Van Westing, E. P. M.; Ferrari, G. M.; de Wit, J. H. W. The Determination of Coating Performance with Impedance Measurements—II. Water Uptake of Coatings. *Corros. Sci.* **1994**, *36* (6), 957−977.
(49) Pérez, C.; Collazo, A.; Izquierdo, M.; Merino, P.; Nóvoa, X. R. Characterisation of the Barrier Properties of Different Paint Systems Part II. Non-Ideal Diffusion and Water Uptake Kinetics. *Prog. Org. Coat.* **1999**, *37*, 169−177.
(50) Perez, C.; Collazo, A.; Izquierdo, M.; Merino, P.; Novoa, X. R. Characterisation of the Barrier Properties of Different Paint Systems. *Prog. Org. Coat.* **1999**, *36* (1−2), 102−108.
(51) Aresta, G.; Palmans, J.; van de Sanden, M. C. M.; Creatore, M. Evidence of the Filling of Nano-porosity in SiO2-like Layers by an Initiated-CVD Monomer. *Microporous Mesoporous Mater.* **2012**, *151*, 434−439.
(52) Gregg, S. J.; Sing, K. S. W. *Adsorption, Surface Area, and Porosity*; Academic Press Inc. Ltd: London, England, 1991.
(53) Rouquerol, J.; Rouquerol, F.; Llewellyn, P.; Maurin, G.; Sing, K. S. W. *Adsorption by Powders and Porous Solids: Principles*; Methodology and Applications Academic Press: 2013.
(54) Sing, K. S. W.; Everett, D. H.; Haul, R. A. W.; Moscou, L.; Pierotti, R. A.; Rouquerol, J.; Siemieniewska, T. Reporting Physisorption Data for Gas/Solid Systems with Special Reference to the Determination of Surface Area and Porosity (Recommendations 1984). *Pure Appl. Chem.* **1985**, *57* (4), 603−619.
(55) Nisato, G.; Bouten, P. C. P.; Slikkerveer, P. J.; Bennet, W. D.; Graff, G. L.; Rutherford, N.; Wiese, L. Evaluating High Performance Diffusion Barriers: the Calcium Test. In *21st Annual Asia Display, 8th International Display Workshop*; 2001; pp 1435−1438.
(56) Nisato, G.; Kuilder, M.; Bouten, P.; Moro, L.; Philips, O.; Rutherford, N. P-88: Thin Film Encapsulation for OLEDs: Evaluation of Multi-layer Barriers using the Ca Test. *Dig. Tech. Pap. - Soc. Inf. Disp. Int. Symp.* **2003**, *34* (1), 550−553.
(57) Goullet, A.; Vallée, C.; Granier, A.; Turban, G. Optical Spectroscopic Analyses of OH Incorporation into SiO2 Films Deposited from O2/Tetraethoxysilane Plasmas. *J. Vac. Sci. Technol., A* **2000**, *18* (5), 2452−2458.
(58) Barranco, V.; Carpentier, J.; Grundmeier, G. Correlation of Morphology and Barrier Properties of Thin Microwave Plasma Polymer Films on Metal Substrate. *Electrochim. Acta* **2004**, *49* (12), 1999−2013.
(59) Dendooven, J.; Devloo-Casier, K.; Ide, M.; Grandfield, K.; Kurttepeli, M.; Ludwig, K. F.; Bals, S.; Van Der Voort, P.; Detavernier, C. Atomic Layer Deposition-based Tuning of the Pore Size in Mesoporous Thin Films Studied by In Situ Grazing Incidence Small Angle X-ray Scattering. *Nanoscale* **2014**, *6* (24), 14991−14998.
(60) Lepoutre, S.; Smått, J.-H.; Laberty, C.; Amenitsch, H.; Grosso, D.; Lindén, M. Detailed Study of the Pore-Filling Processes During Nanocasting of Mesoporous Films Using SnO2/SiO2 as a Model System. *Microporous Mesoporous Mater.* **2009**, *123* (1−3), 185−192.
(61) Boissiere, C.; Grosso, D.; Lepoutre, S.; Nicole, L.; Brunet-Bruneau, A.; Sanchez, C. Porosity and Mechanical Properties of Mesoporous Thin Films Assessed by Environmental Ellipsometric Porosimetry. *Langmuir* **2005**, *21* (26), 12362−12371.
(62) Bourgeois, A.; Brunet-Bruneau, A.; Fisson, S.; Rivory, J.; Matheron, M.; Gacoin, T.; Boilot, J. Adsorption and Desorption Isotherms at Ambient Temperature Obtained by Ellipsometric Porosimetry to Probe Micropores in Ordered Mesoporous Silica Films. *Adsorption* **2005**, *11* (S1), 195−199.
(63) Mansfeld, F.; Shih, H.; Greene, H.; Tsai, C. H. Analysis of EIS Data for Common Corrosion Processes. In *Electrochemical Impedance: Analysis and Interpretation*; American Technical Publishers LTD: 1993; pp 37−53.
(64) Deflorian, F.; Fedrizzi, L.; Rossi, S.; Bonora, P. L. Organic Coating Capacitance Measurement by EIS: Ideal and Actual Trends. *Electrochim. Acta* **1999**, *44*, 4243−4249.
(65) Aranovich, G. L.; Donohue, M. D. Diffusion in Fluids with Large Mean Free Paths: Non-Classical Behavior Between Knudsen and Fickian Limits. *Phys. A* **2009**, *388* (17), 3355−3370.

DOI: 10.1021/acsami.5b04060
ACS Appl. Mater. Interfaces 2015, 7, 15968−15977